Optical Detection of Electron Spin Resonance in Fluorescent Microdiamonds

Yunki Yau[1,*]

[1] *SID 200491720, SCDL3991 Semester 1, 2025*

(Dated: June 23, 2025)

Negatively charged nitrogen-vacancy (NV^-) centres in diamond are exceptionally stable quantum systems that exhibit spin-dependent photoluminescence under ambient conditions, and their low hardware requirements make them highly promising for integration into solid-state devices for quantum sensing applications. Herein we present a prototype optical system for detecting the Electron Spin Resonance (ESR) of microdiamond (NV^-) centres. Our compact setup integrates laser excitation and photon detection with microwave and magnetic field control to resolve both zero-field and Zeeman-split spin sublevels. Our results demonstrate that even with a modest setup, we can exert and observe quantum effects in solid-state systems.

I. BACKGROUND

Negatively-charged Nitrogen-vacancy (NV^-) centres are naturally occurring atomic-scale defects in diamond with remarkable optically detectable magnetic resonance (ODMR) properties [1]. With developments in precision fabrication techniques, NV^- centres have been the subject of intense interest for their potential application as quantum processors and sensors [1, 2].

NV^- defects are formed by a Nitrogen (N) atom replacing two Carbon (C) atoms in a diamond lattice that results in a lattice vacancy coupled to the N atom [3]. Within the defect complex, after all available covalent bonds are formed, six defect electrons (including an electron donated by the lattice) remain, forming a spin triplet ($S = 1$) ground state that can be understood as a system of two unpaired electrons [3]. Excitation of this ground state into the first excited state preserves the spin state of the system, which consists of the $|m_s = 0\rangle$ and $|m_s = \pm 1\rangle$ eigenstates (FIG. 1).

Excited-state $|m_s = 0\rangle$ populations predominantly undergo radiative decay to the ground state, emitting fluorescence at 637 nm [1]. In contrast, the $|m_s = \pm 1\rangle$ excited states exhibit a significant probability of non-radiatively decaying via intermediate singlet states $|^1A_1\rangle$ and $|^1E\rangle$, returning to the ground $|m_s = 0\rangle$ state through a spin-forbidden transition known as intersystem crossing (FIG. 1) [4].

A key property that makes the NV^- centre viable for quantum information processing is the ability to optically initialise and manipulate its spin state: $|m_s = 0\rangle$ and $|m_s = \pm 1\rangle$ eigenstates have a zero-field energy splitting of 2.87 GHz and coherent transitions between them can be driven by resonant microwave excitation (FIG. 1). In diamond, the degeneracy of the $|m_s = \pm 1\rangle$ sublevels is lifted by local lattice strain [3]. This $|m_s = \pm 1\rangle$ splitting can be further accentuated through the Zeeman effect by application of an external magnetic field, which can enable better spectral resolution of the NV^- centre spin sublevels [3, 5]. Together, this allows full optical detection of the NV^- centre's spin triplet structure.

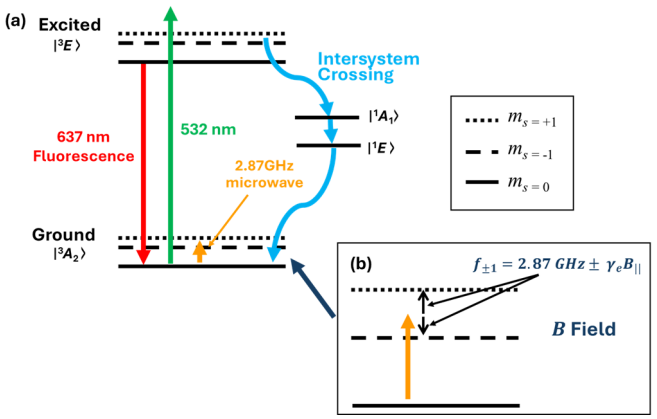

FIG. 1. Energy level structure and optical transitions of NV^- centres in diamond. (a) The ground-state spin triplet ($^3A_2$) can be optically pumped off-resonance to the excited-state triplet (^3E) using a 532 nm green laser. Resonant microwave excitation at 2.87 GHz enables coherent transitions from ground-state $|m_s = 0\rangle$ to $|m_s = \pm 1\rangle$ spin states. The $|m_s = \pm 1\rangle$ sublevels preferentially decay via intersystem crossing into the $|m_s = 0\rangle$ ground state, polarising the spin population. (b) In an external magnetic field B, the $|m_s = \pm 1\rangle$ states experience Zeeman splitting, and their transition frequencies are given by $f_{\pm 1} = 2.87\ \text{GHz} \pm \gamma_e B_{||}$, where γ_e is the electron gyromagnetic ratio and $B_{||}$ is the magnetic field component along the NV axis [6, 7].

In this study, we aimed to design and construct a prototype photodetection platform to detect the Electron Spin Resonance (ESR) of NV^- centres in micro-diamonds using standard optomechanical and microwave components. The primary experimental objectives were to:

- Develop an optical setup for initializing the spin state of NV^- centres in micro-diamonds using laser excitation.
- Detect and characterise the intrinsic zero-field spin transition near 2.87 GHz.
- Resolve the Zeeman splitting of the $|m_s = \pm 1\rangle$ spin sublevels under an applied magnetic field.

* yyau2516@uni.sydney.edu.au

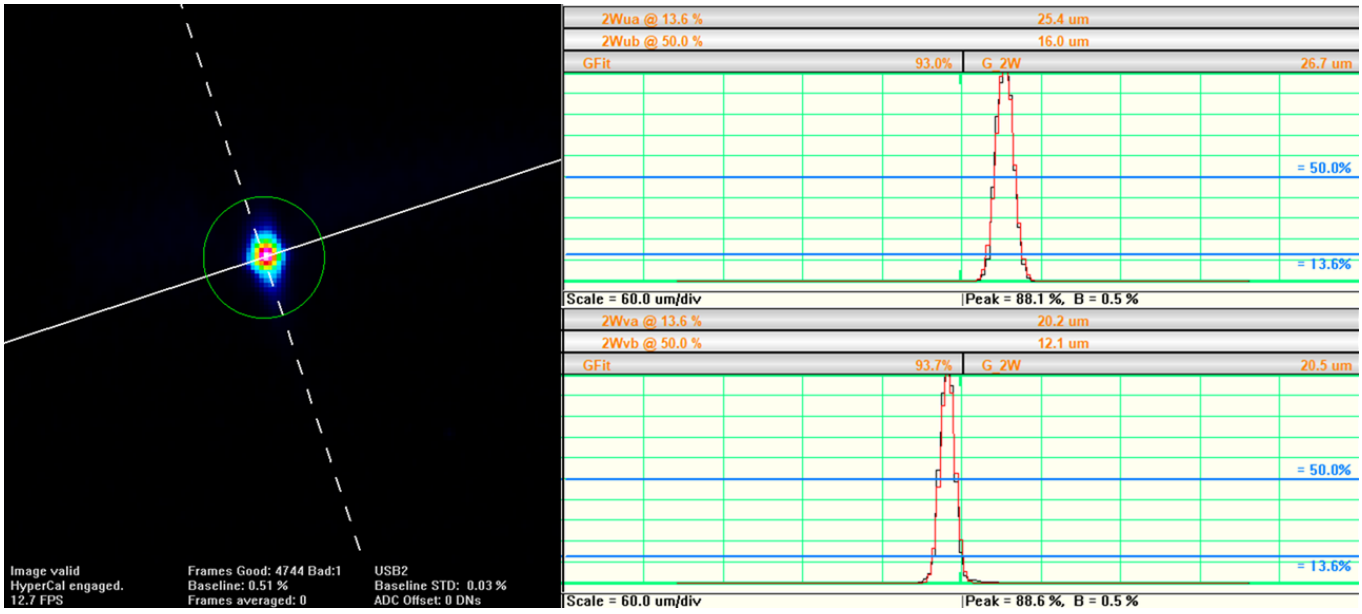

FIG. 2. Intensity profile of the focused excitation laser. The beam profile was measured using the BladeCam2-XHR camera and DataRay Beam Profiling software (v8.0D36, DataRay Inc, USA). The right-side of the image shows the gaussian fits of the major (u) and minor (v) axes, which measured 16.0 µm and 12.1 µm at FWHM, respectively.

II. METHODS

A. Microdiamond sample preparation

15 µm diameter red fluorescent microdiamond powder (3.5 ppm NV^-) (Adámas Nanotechnologies, USA) were drawn up from a microcentrifuge tube using a syringe and blunt-tip needle and aspirated onto a drop of ethanol on a 80 µm glass cover slide. The glass slide was then dried on a heat plate prior to use.

B. Construction of Optomechanical Layout

The experimental setup of the photodetection system is shown in FIG. 3. A 532 nm PL520 diode laser (5 V) was directed through a set of aspherical and cylindrical beam-shaping optics. Significant iterative beam conditioning was required to correct for the diode's inherent astigmatism and elliptical output, and to produce a well-collimated, near-circular Gaussian beam. This process involved fine adjustment of inter-lens distances and angular alignment, and was validated through repeated beam profiling measurements (FIG. 2. The conditioned beam was then reflected off a 605 nm longpass dichroic mirror and focused onto the microdiamond sample using a 0.5 NA, $f = 8.00$ mm lens producing a sub-20 µm focus (FIG. 2).

Red fluorescence emitted isotropically from the illuminated diamond was recollected through the same focusing lens, filtered by a 561 nm longpass filter, and coupled into a multimode optical fibre. Precise alignment of the fibre coupler with respect to the emission cone was essential for maximizing signal capture, and iterative adjustments to the angular tilt and longitudinal position of the fibre port were performed to optimize coupling efficiency, assessed in real-time by photon count rate. Initially, photon collection was performed using a SPCM20A Single Photon Counting module (Thorlabs, USA). However, early measurements yielded photon count rates below 1000 counts/s, suggesting suboptimal excitation or poor emission capture.

Achieving optimal optical pumping of NV^- centres required micron-level alignment of the laser focus onto individual microdiamonds distributed on a glass slide. By incrementally scanning the laser focus across the sample plane, we eventually achieved direct illumination of a single fluorescent microdiamond. This resulted in a dramatic increase in signal intensity—photon counts by over four orders of magnitude, exceeding 1×10^7 counts/s. At this point, the fluorescence was visibly detectable by eye through the optics. Owing to this high signal regime, the detector was switched from a Single Photon Counter to a photodiode to accommodate the increased light flux and broaden the dynamic range.

All optomechanical components, including mounts, stages, and coupling elements, were sourced from Thorlabs (USA) and Schäfter+Kirchhoff (Germany).

C. Microwave Control and Synchronised Data Acquisition

Microwave frequencies ranging from 2.5 to 3.2 GHz were generated using an SG4400L compact RF Signal

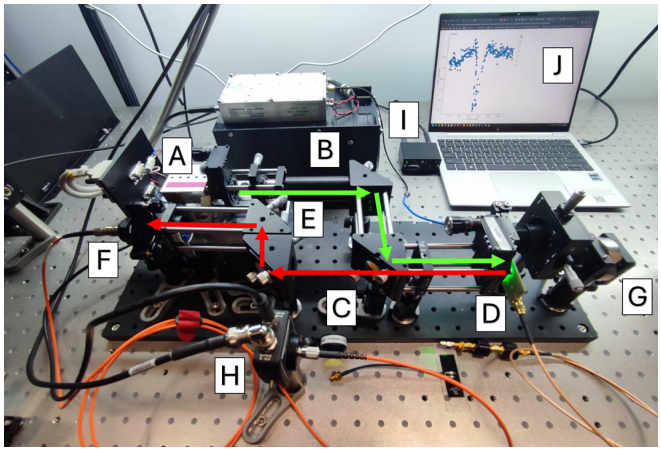

FIG. 3. Setup of photodetection system on the optical bench. The green arrows indicate the excitation laser path and the red arrows indicate the path of the diamond fluorescence captured in the system. Components are labelled as follows: A) 532nm laser diode in prefabricated housing. B) Laser mirror system. Beam-shaping optics are on the left of the laser tube. C) 605nm dichroic mirror. D) High-NA focusing lens and diamond sample on PCB board. E) Fluorescence mirror system. F) Optical fibre collimator G) Neodymium magnet mounted on optomechanical holder. H) Photodiode I) Microwave frequency generator with amplifier on the left. J) Control computer running a custom Python script to synchronise photodetection and frequency scanning bins.

Generator (DS Instruments, USA) in 1 MHz bins for 100 ms. 15 dBm microwaves were delivered via a 5W amplifier connected to a custom transmission stripline on a printed circuit board, and the micro-diamond slide was glued face down directly over the stripline to maximise incident microwave power on the sample. A neodymium ring magnet provided a static external magnetic field, which was placed 8, 9 and 12 cm away from the micro-diamond sample equating to field strengths of 0.8, 1.8 and 2.6 mT.

Photoluminescence intensity was recorded using a photodiode connected to a digital oscilloscope (Liquid Instruments, Australia). A custom Python control script was specifically developed for this experiment to automate and synchronise microwave frequency sweeping with photodiode voltage acquisition. The system interfaced with both the SG4400L and the oscilloscope using serial communication via the `pyserial` and `pymoku` libraries, while data processing and visualization were handled using `numpy` and `matplotlib`.

For each frequency point, the script recorded photodiode voltages with the microwave source toggled on and off in sequence, and their ratio was taken to normalise for fluctuations in laser intensity.

III. RESULTS

A. Zero-field Splitting

Applying a microwave frequency scan from 2.5 to 3.2 GHz in the absence of the neodymium magnet component, we observed 2.6 - 3 % contrasts in photoluminescence intensity at 2.863 and 2.875 GHz (FIG. 4, Table I). The Full Width Half-Maximum (FWHM) of these minima were on the order of tens of MHz.

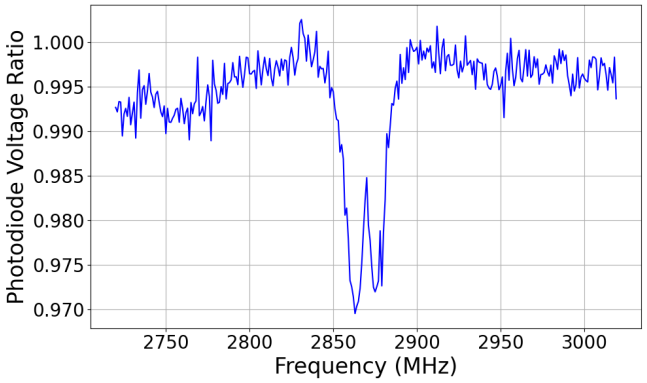

FIG. 4. Trace of zero-field splitting between $|m_s = 0\rangle$ and $|m_s = \pm 1\rangle$ spin sublevels in microdiamond NV^- centres. Two distinct resonance dips are observed at 2.863 GHz and 2.875 GHz, symmetrically offset by approximately 6 MHz from the zero-field resonance.

B. Zeeman Splitting

To probe Zeeman splitting of the $|m_s = \pm 1\rangle$ spin sublevels, the 2.5 to 3.2 GHz microwave frequency sweep was performed under external magnetic fields of 0.8, 1.8, and 2.6 mT, as previously mentioned.

As shown in FIG. 5, each applied magnetic field resulted in two photoluminescence minima approximately symmetrically offset from the zero-field resonance near 2.87 GHz. Photoluminescence contrasts decreased from 3 % at zero-field to 1.3 - 2.0 % under applied fields (Table I). The resonance separation $\Delta f = f_{+1} - f_{-1}$ also increased approximately linearly with applied field, from 12 MHz at zero field to 83 MHz at 2.6 mT (FIG. 6, Table I).

IV. DISCUSSION

The results presented here demonstrate the effectiveness of a compact, accessible platform for detecting electron spin resonance in NV^- centres. Using standard optomechanical and RF components integrated via custom Python control, our system achieved micron-level laser

TABLE I. Observed Zeeman resonances and photoluminescence contrasts under varying magnetic field strengths. Center frequencies f_{-1} and f_{+1} were estimated by manually identifying the minimum photodiode voltage within selected frequency windows. Uncertainties reflect half the 1 MHz microwave step size.

Magnetic Field (mT)	$f_{-1} \pm 0.5$ **(MHz)**	$f_{+1} \pm 0.5$ **(MHz)**	$\Delta f = f_{+1} - f_{-1}$ **± 1 (MHz)**	**Photoluminescence Contrast ± 0.3 (%)**
0.0	2863	2875	12	3.0
0.8	2857	2875	18	1.7
1.8	2838	2898	60	2.0
2.6	2827	2910	83	1.3

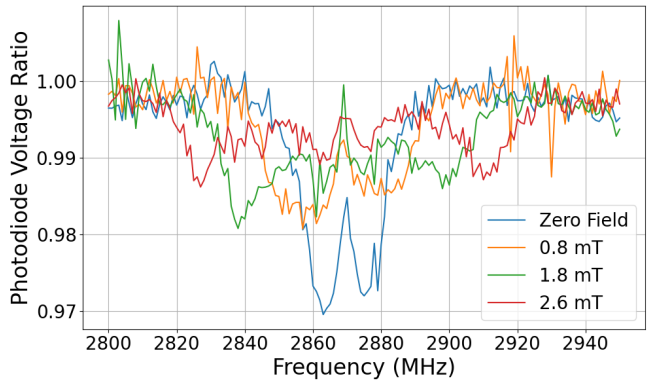

FIG. 5. Zeeman splitting of $|m_s = \pm 1\rangle$ spin sublevels in microdiamond NV$^-$ centres under zero and varying magnetic field strengths. FWHM of each minimum are 20 MHz.

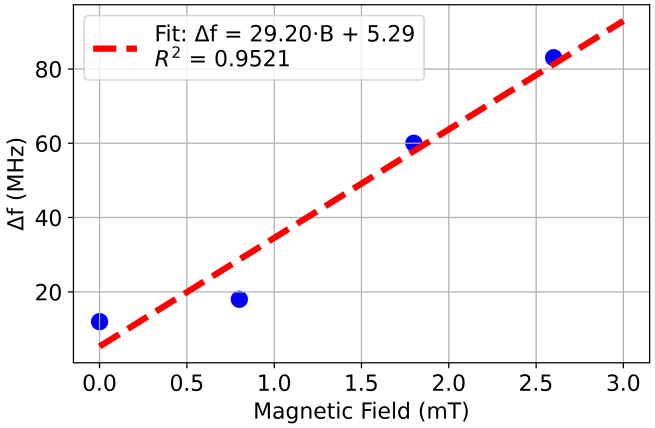

FIG. 6. Resonance separation ($\Delta f = f_{+1} - f_{-1}$) vs magnetic field strength. The linear fit yielded a coefficient of determination $R^2 = 0.95$, indicating a strong correlation consistent with Zeeman splitting.

focus that allowed efficient optical pumping of NV centres and synchronization of microwave delivery and photodetection. This enabled optical differentiation of zero-field and Zeeman-split NV$^-$ centre spin sublevels with photoluminescence decreases resolved with contrasts of up to 3% (FIG. 5, Table I). We further observed a positive linear correlation between the frequency separation Δf and magnetic field strength (FIG. 6, and decreased photoluminescence contrasts in the presence of external magnetic fields, consistent with theoretical and published expectations [5, 8].

Notably, two distinct minima were observed ±6 MHz around the resonant 2.87 GHz frequency in the zero-field setting. This is due to mechanical lattice strain, an established characteristic of the NV$^-$ system [3, 6, 9]. In fact, the physical characteristics of diamond, including lattice strain, interstitials, and surface defects, make them difficult to precisely characterise and remain significant standing challenges to their application as qubits in quantum computing architectures [2, 3].

An alternative argument for the zero-field splitting observed is the presence of stray magnetic fields in the experimental environment. The setup presented here was constructed within the confines of an ion trap laboratory with strict magnetic field monitoring and control, and a simple calculation of the magnetic field strength that would cause the observed zero field splitting (if not due to lattice strain) equates to 0.03 mT, which is within the range of Earth's geomagnetic background. In addition, the reduction in photoluminescence contrasts we observed under applied magnetic fields further suggests that the zero-field splitting we observed is orientation-independent, which is consistent with lattice strain effects.

When we performed the microwave frequency sweep in the presence of an external magnetic field, the frequency separation Δf increased linearly with field strength, consistent with the Zeeman effect (FIG. 6) [6, 7]. The reduced contrast compared to the zero-field setting was also an expected outcome and can be attributed to the broadening of the ODMR spectrum due to angular dependence of the orientation of individual NV$^-$ centres with the applied magnetic field [6]. Given that each microdiamond contains on the order of 10^6 NV centres, the resulting ensemble average leads to a smearing of the resonance features and decreased resolution of the ESR signals. This could potentially be improved by averaging multiple repeated frequency sweeps or using longer interrogation times to improve signal-to-noise ratios.

A. Future Work

We aim to build on our ability to resolve NV^- spin resonances demonstrated here by incorporating an RF Paul trap in our photodetection system to levitate and precisely control microdiamonds. Removing physical contact with a solid substrate — such as a glass slide — helps mitigate localised strain and charge interactions, both of which can degrade spin coherence and decrease spectral resolution [5, 10, 11]. In addition, levitation and the open geometry of a Paul trap reduces substrate-related laser heating and facilitates more flexible fluorescence collection options, which would improve thermal stability of the system and enhance its sensitivity for ODMR measurements.

V. CONCLUSION

In this study, we have designed and built a fully custom, compact ESR detection platform capable of resolving both zero-field and Zeeman-split spin transitions in NV^- centres embedded in fluorescent microdiamonds. The entire optical, microwave, and photodetection system was designed and implemented from the ground up, including bespoke synchronised control of hardware components and data acquisition. Our results show that even with modest resources, it is possible to exert quantum control over solid-state spin systems, making it well-suited for educational demonstrations and accessible quantum sensing experiments. Looking forward, the path is now open for finer spatial and spectral control using ion trapping techniques. The work presented here provides a foundational step toward a scalable quantum education platform.

ACKNOWLEDGMENTS

I extend my sincere thanks to Dr. Robert Wolf and Dr. Cyril Laplane at the University of Sydney Quantum Control Laboratory for their supervision and friendship during this project.

[1] V. Acosta and P. Hemmer, MRS bulletin **38**, 127 (2013).
[2] R. Katsumi, K. Takada, F. Jelezko, and T. Yatsui, Communications Engineering **4**, 1 (2025).
[3] A. Haque and S. Sumaiya, Journal of Manufacturing and Materials Processing **1**, 10.3390/jmmp1010006 (2017).
[4] H. Duarte, H. T. Dinani, V. Jacques, and J. R. Maze, Phys. Rev. B **103**, 195443 (2021).
[5] T. Delord, L. Nicolas, L. Schwab, and G. Hétet, New Journal of Physics **19**, 033031 (2017).
[6] M. W. Doherty, N. B. Manson, P. Delaney, F. Jelezko, J. Wrachtrup, and L. C. Hollenberg, Physics Reports **528**, 1 (2013).
[7] D. J. Griffiths and D. F. Schroeter, *Introduction to Quantum Mechanics*, 3rd ed. (Cambridge University Press, 2018).
[8] A. Kuhlicke, A. W. Schell, J. Zoll, and O. Benson, Applied Physics Letters **105** (2014).
[9] J. R. Maze, A. Gali, E. Togan, Y. Chu, A. Trifonov, E. Kaxiras, and M. D. Lukin, New Journal of Physics **13**, 025025 (2011).
[10] K. W. Lee, D. Lee, P. Ovartchaiyapong, J. Minguzzi, J. R. Maze, and A. C. Bleszynski Jayich, Physical Review Applied **6**, 10.1103/physrevapplied.6.034005 (2016).
[11] M. Kim, H. J. Mamin, M. H. Sherwood, K. Ohno, D. D. Awschalom, and D. Rugar, Phys. Rev. Lett. **115**, 087602 (2015).